Gas-phase materials synthesis in environmental transmission electron microscopy

Kimberly A. Dick

Gas-phase transmission electron microscopy is an essential tool for elucidating the mechanisms involved in the synthesis of functional materials. Here, we review the latest developments in understanding the growth of novel nanostructural materials afforded by following the process *in situ* in electron microscopes. Particular focus is on investigations of catalyzed growth of one-dimensional carbon-based and semiconductor nanostructures, while other types of nanocrystal and epitaxial crystal growth are briefly addressed. Also discussed are how these methods have been employed to answer critical questions about the growth mechanisms as well as to bring insight into the relationships between synthesis parameters and materials properties.

Introduction

The development of the gas-phase transmission electron microscope—environmental transmission electron microscopy (ETEM)—has opened up a plethora of opportunities to study dynamic processes in material formation, transformation, and dynamics under realistic conditions. The introduction of gas to a sample while it is imaged by transmission electron microscopy (TEM) allows us to identify *in situ* the kinetics of transformation processes, phases involved, and dynamics by which the processes occur.[1] If the environment can be varied in a controlled way during the imaging process and the temperature controlled, a remarkable depth of information can be attained that few other methods can offer. Some of the most complex processes that can be investigated in ETEM involve the synthesis of materials, including nucleation and crystal growth. Synthesis and crystal growth processes are of central importance to all types of material development but involve complex thermodynamic and kinetic processes that are difficult to unravel by most experimental techniques. Developments in ETEM and *in situ* TEM thus provide exciting and unparalleled opportunities to address important questions in materials synthesis.

Some of the earliest *in situ* investigations of materials synthesis inside a TEM involved a reaction of solid samples with trace gas species in the vacuum, such as the oxidation of Si from oxygen and/or water residues.[2] Gas-phase experiments can, in principle, also be conducted by local evaporation (and subsequent redeposition) of a solid precursor by the electron beam. More advanced and controlled experiments are made possible by the development of instruments into which precursor gases for solid material growth can be introduced.[3,4] However, *in situ* investigations of crystal growth and nucleation only became widespread with the development of liquid cell holders. Liquid cell holders enclose a droplet containing precursors for a solution-phase synthesis, allowing the nucleation process and subsequent growth stages to be visualized directly. A very wide range of materials have been studied, including metal nanoparticles, compound ceramic materials as well as ice and proteins. A thorough review of recent *in situ* TEM investigations of nucleation and crystal growth mechanism with focus on liquid cell experiments is presented in Reference 5.

Compared to liquid cell experiments of crystal growth and synthesis, gas-phase experiments offer significant advantages in terms of resolution, complementary *in situ* analysis methods (such as energy-dispersive x-ray spectroscopy [EDX], for identifying the elements present in a growing crystal in real time), and controllable/reversible switching of environment (compared to liquid experiments, where the liquid composition can change over time). Although nucleation and subsequent

Kimberly A. Dick, Centre for Analysis and Synthesis, Lund University, Lund, Sweden; kimberly.dick@ftf.lth.se
doi:10.1557/s43577-023-00579-4

crystal evolution can be followed just as in a liquid cell, the process is fundamentally different in that spent reactant gases are continually removed and fresh precursor species pumped in. In this way, the effect of the reactive environment can be monitored in a continuous way, allowing for more extensive studies of the relationship between the synthesis process and the product.

Gas-phase synthesis experiments have become much more common with the development of closed-cell gas holders, but also rapid improvements in dedicated ETEM capabilities that allow for more realistic conditions to be reached, including in aberration-corrected microscopes (the development of gas-phase TEM is discussed in Reference 6). Compared to liquid cell experiments, a more extensive and complex apparatus is required to handle precursor gases. Of the wide range of crystals that can be grown, most gas systems are designed to handle only simple gases, and studies of, for instance, oxidation vastly outnumber all other types of synthesis (compare to liquid, where a wide range of precursors can be chosen to enclose within the cell). Commercially available closed-cell gas holders are becoming particularly common because they can be integrated with a range of microscope types rather than requiring a dedicated system. They also typically allow for higher maximum pressures than dedicated (i.e., open-cell) ETEMs, because the gas species never enter the microscope column. On the other hand, dedicated ETEMs typically offer the highest achievable spatial resolution (with fewer obstacles in the beam path) and are more compatible with complementary analysis tools such as EDX.[7]

Gas-phase synthesis and crystal growth experiments per definition require a net deposition of species from the vapor to the solid phase. This means that gas-phase synthesis typically poses additional technical challenges compared to many other *in situ* or *operando* gas-phase experiments (such as in References 8 and 9)—essentially, gas species and reaction conditions are chosen to favor deposition, which means that contamination must always be addressed. In a closed-cell gas holder, deposition could occur within the gas cell and gas lines, making it difficult to fully remove a species and change to another gas. Open-cell configurations typically benefit from increased pumping capacity and reduced flow limitations (waste gas does not need to be removed via narrow lines); however, deposition can occur on other components in the polepiece area and other parts of the microscope. Despite these challenges, continuous technical developments have enabled a rapidly expanding range of gas-phase synthesis experiments.

In this article, the background and latest development in gas-phase synthesis of materials in environmental and *in situ* TEM will be discussed. The focus will be on the synthesis of novel nanocrystals, which are inherently well-suited to ETEM investigation due to their nanoscale dimensions. The most well-studied categories of nanostructures are one-dimensional (1D) structures promoted by a metal catalyst (carbon-based and semiconducting nanotubes, nanofibers, and nanowires). These will be discussed in Sections "Catalytic synthesis of 1D carbon nanostructures" and "Growth of semiconductor nanowires." These are followed by shorter discussions of nanocrystals formed by gas–solid transformations, and epitaxial growth of nanocrystals on crystalline and 2D substrates.

Catalytic synthesis of 1D carbon nanostructures

Some of the most well-studied types of nanostructures synthesized using gas-phase electron microscopy are carbon nanotubes (CNTs) and related carbon nanostructures (**Figure 1**). Interest in CNTs soared after their discovery in 1991[10] owing to their unique and unprecedented electrical and mechanical properties. Some of the earliest *in situ* investigations were reported just over a decade later, giving direct visualization of the growth process of single and multi-walled CNTs[11,12] and insight into the effect of environment on growth kinetics.[13] CNTs are most commonly (and controllably) synthesized using a catalyst (most often Fe, Co or Ni, although other metals are also used), which is exposed to a gas species such as methane, propylene, acetylene, or ethylene. Nucleation of the carbon-based structure at the catalyst surface initiates the CNT formation, and continuous growth occurs so long as the gas species remains.

With extensive and rapid development of CNT growth processes occurring following their discovery, ETEM experiments have been essential to understanding the growth mechanisms.[14] ETEM experiments have focused on understanding the formation mechanisms of the catalyst particles,[15,16] and given insights into the nucleation of carbon structures in the early stages of growth.[17,18] The roles of catalyst morphology and dynamics in driving these early stages of the growth process have also been reported.[19,20] For the subsequent growth process, some of the most important questions to be addressed involve the phase and structure of the catalyst—specifically, whether it is crystalline, liquid, amorphous, or a combination/fluctuation between phases. For crystalline phases, it is also of interest to know specifically which crystal structures are active, and how this affects properties such as chirality. Other questions relate to the growth mechanism in general, and whether all classes of catalyzed CNT growth can be understood by the same principles. Transport pathways of carbon are also of interest—for instance, does it diffuse through or along the catalyst, and by what pathways?

An early *in situ* TEM study of Fe-catalyzed CNT growth reported that crystalline Fe_3C was the active catalyst phase during growth.[21] In contrast, a later study concluded that the partial melting of Fe_3C played a role in the CNT growth process.[22] The same paper reported that Au catalysts for CNT growth are metallic and fluctuate between crystalline and quasi-liquid phase. Feng et al.[23] also proposed that a liquid-like state plays a general role in catalyzed CNT growth. Indeed, a complex quasi-liquid surface phase surrounding a metastable carbide phase of Ru catalyst particles was reported to drive the formation of "fishbone-like" 1D carbon nanostructure growth.[24] Other studies conclude that at least some

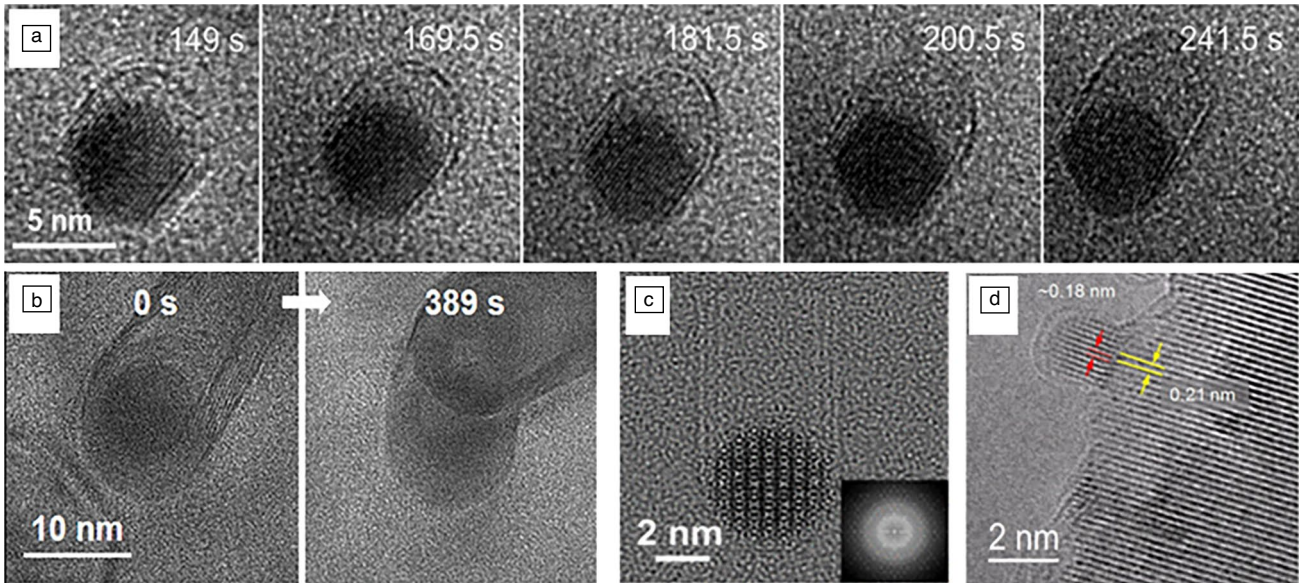

Figure 1. Carbon nanotube (CNT) growth studied *in situ*. (a) Formation of a CNT from a Pt catalyst. Reprinted with permission from Reference 38. © 2022 American Chemical Society. (b) CNT growth from a Co-based catalyst. Reprinted with permission from Reference 32. © 2020 American Chemical Society. (c) Growth of a multi-walled CNT from a Co-W–C particle. Reprinted from Reference 40 under Creative Commons CC BY license. (d) Early-stage formation of a carbon cap on Co nanoparticle catalyst. Reprinted from Reference 37 under Creative Commons CC BY license.

types of catalyst particles are fully crystalline during growth: One study reported that either metallic Fe or Fe_3C could act as a catalyst for CNT growth depending on growth parameters.[25] Another study directly compared Fe_3C and Fe_5C_2 catalysts for CNT growth and found that only Fe_3C was active.[26] Although single-phase particles are typically reported for Fe-catalyzed growth, it was reported that Co-based catalysts contained a mix of Co carbide and metallic phases during the growth process.[27] Ni-based catalysts are more often reported to exhibit a metallic phase during growth.[12,28,29]

Although nanoparticle phase and structure have been studied *in situ* for nearly two decades, the development of aberration-corrected ETEMs with higher pressure and temperature capabilities has led to a resurgence of studies focused on these questions in recent years. In particular, there has been a renewed interest in addressing the apparent disagreements about the phase and active structure of CNT catalysts (potentially a result of differing experimental conditions, which may not have represented more conventional growth conditions).[30] In particular, it has been suggested that observations of the metallic phase were a consequence of the low pressures of C-containing precursors used in these studies. A recent *in situ* TEM study of Fe-catalyzed CNT growth under realistic conditions with high resolution concluded that the catalyst consists of a solid Fe_3C nanoparticle, which behaves in a highly dynamic way, potentially indicating fluctuating C content during growth.[30] A similar study found the analogous Ni_3C structure to be the active phase for Ni-catalyzed growth of carbon nanofibers (CNFs).[31] For Co-catalyzed CNT growth, more significant controversies have been attributed to the multiple carbides present in this system, which are difficult to distinguish due to their similar lattice spacings. A recent *in situ* TEM study with high resolution and near-atmospheric conditions, however unambiguously, assigned the phase during CNT growth to Co_3C.[32] This study further explored the diffusion kinetics of C through the catalyst.

Further insights into the catalytic growth mechanism were afforded by a study demonstrating that structural fluctuations inside the catalyst for Co-catalyzed CNT growth play a key role in the process.[33] They also address the mechanism of C atom transport to the interface, indicating that both surface diffusion and diffusion from the bulk are important. It was also reported that the shape and faceting of the catalyst are directly connected to the mechanism for multi-walled CNT growth, with the formation of graphene layers on specific facets acting as the first stage in CNT shell formation.[34] Another study explored how the Co-catalyzed CNT growth process can be terminated and then a new CNT initiated.[35] More recently, a detailed investigation of the interfacial processes between Co-based catalyst and the growing CNT elucidated the role of interfacial interaction in determining the nanotube morphology.[36]

ETEM experiments with high resolution and high pressure have also enabled studies of the growth of CNTs in more uncommon and complex systems. In another study, the growth mechanism of CNFs was explored for bimetallic Ni–Co catalysts, which are understood to have superior activity to monometallic catalysts.[39] Understanding the mechanism of bimetallic catalysis and its relationship to catalyst phase and structure is even more challenging, but necessary, for understanding their performance. Interestingly, the active structure was found to be a metallic phase rather than the

carbides observed for typical monometallic catalysts under realistic pressures, which could explain the superior activity. The feasibility of controlling structure with a bimetallic catalyst was however questioned by an *in situ* study of Co–W alloy catalysts, which concluded that the varying structural relationship between catalyst and CNT would make this very challenging.[40]

In addition to understanding growth mechanisms at a fundamental level, identifying means to control the properties of the resulting nanostructure is a central aim for ETEM studies. One early study proposed that engineering of the catalyst phase or structure could be used to control chirality of the growing CNT.[28] This was demonstrated more directly for *in situ* growth of CNT growth from metallic Co nanoparticles, which reported a high selectivity for specific chiralities as a consequence of catalyst structural matching, which could be tuned with growth temperature.[37] Growth from Pt nanocatalysts with defined facets was also explored *in situ as* a means to control chirality of the grown CNT.[38] It was found that the nucleation of the nanotube was facet-dependent in the early stages, such that control of nucleation could be possible by control of nanoparticle faceting.

Growth of semiconductor nanowires

One-dimensional semiconductor nanowires can be grown by a metal-catalyzed process that is conceptually similar to that observed for CNT. Catalyzed growth of 1D semiconductors is considered a promising means to tailor electronic, optical, and mechanical properties, yielding novel materials of interest for electronics, photonics, and energy conversion.[41–43] The mechanism by which these nanowires grow and the dynamic processes that control the relationship between growth parameters and resulting materials properties are, however, quite complex. ETEM has therefore emerged as an important tool for addressing fundamental questions in the growth mechanism, as well as identifying novel phenomena and new means to control the growth process.[44] The first demonstration of *in situ* growth of semiconductor nanowires was reported in 2001.[45]

The most common catalyst used for semiconductor nanowire growth is a Au nanoscale droplet, which forms a low-temperature eutectic alloy with the semiconductor element(s). These materials are typically grown from gas-phase precursor species; as such, the mechanism is often termed vapor–liquid–solid (VLS), for the phases of the supply, catalyst, and nanowire. The analogous process using a solid catalyst, as typically observed for CNTs, is termed vapor–solid–solid (VSS). In addition to determining the catalyst phase, other important questions involve the relationship between growth dynamics and resulting nanowire properties such as morphology, crystal structure, and composition.

Extensive *in situ* investigations of Si and Ge nanowire growth have provided important insights into nanowire growth mechanisms, and demonstrated new, unexpected phenomena. For Au-catalyzed Si nanowires, the dynamic stability of the Au droplet and its role in determining nanowire properties such as diameter[46] and morphology were explored. It is shown that the size of the nanowire can vary as a consequence of out-diffusion of Au atoms from the droplet,[47] which can be controlled by introducing oxygen to passivate the surface (**Figure 2**a).[48] The effect of droplet dynamics in determining nanowire morphology was also established to account for instance for sawtooth faceting[49] and nanowire kinking.[50,51]

The phase of the droplet (or nanoparticle) was also established to address a long-standing controversy. Just as for CNTs, one of the central questions for nanowire growth prior to *in situ* observation related to the phase of the catalyst (solid or liquid, and with what structure and composition). It was demonstrated *in situ* that both VLS and VSS processes are possible for Au-seeded Ge nanowires, depending on growth conditions and growth history,[52] while VSS processes are common with a range of other catalyst metals such as Pd, Al, and Cu (Figure 2b).[53–55] The kinetics of individual nucleation events initiating nanowire growth and mechanistic pathways were also established for both VSS and VLS processes.[56,57]

Before *in situ* observations were available, it was hypothesized that VLS nanowire growth occurs in a layer-by-layer

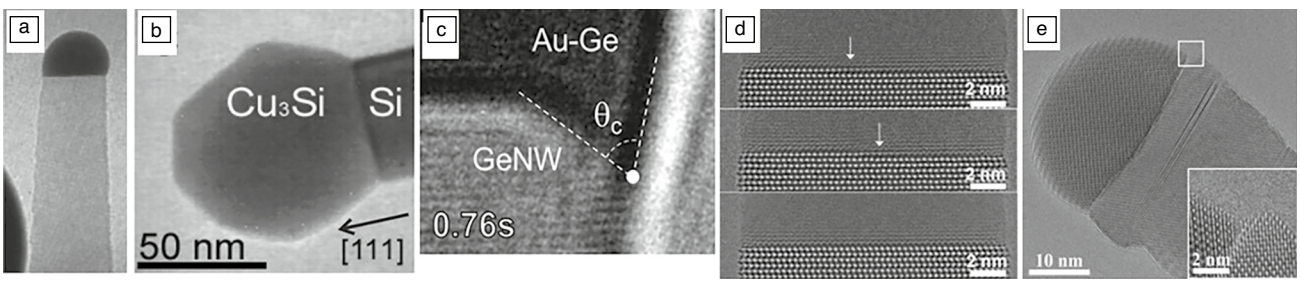

Figure 2. *In situ* growth of semiconductor nanowires. (a) Example of Au-catalyzed Si nanowire. Reprinted with permission from Reference 48. © 2006 American Chemical Society. (b) Si nanowire growth catalyzed by a solid Cu_3Si nanoparticle. Reprinted with permission from Reference 54. © 2010 American Chemical Society. (c) Observation of dynamic truncated interface in Ge nanowire growth. Reprinted with permission from Reference 61. © 2011 American Chemical Society. (d) Observation of layer growth in a GaAs nanowire. Courtesy of K. Kumar. (e) Example of GaP nanowire growth catalyzed by a solid Cu nanoparticle. Adapted with permission from Reference 71 under Creative Commons CC BY license.

fashion, in which precursor species accumulate in the droplet during an incubation period, followed by a single nucleation event and subsequent growth at the droplet–nanowire interface. This mechanism was substantiated by *in situ* experiments clearly showing an incubation period during which no growth occurred, followed by formation of a single complete layer; the actual nucleation and layer growth processes were however too rapid to observe.[58,59] VSS growth dynamics are found to be slightly different: layer growth is much slower and readily observable, but the incubation process is rapid, such that a new layer starts to grow immediately after the previous one is completed.[54,55,58] The difference in growth dynamics was attributed to the much higher concentration of growth species required to supersaturate a droplet versus a solid; this understanding was further utilized to demonstrate a method to control interface structure in Ge-Si heterostructure nanowires, by changing the nanoparticle phase.[53]

Finally, *in situ* observations demonstrated that while the classical view of incubation, nucleation, and layer growth is generally valid, the interface between the droplet/nanoparticle and nanowire is often much more dynamic. A highly active "truncation" was in many cases observed at the perimeter of the droplet–nanowire interface, and sometimes observed to fluctuate in response to the formation of layers—giving a different growth dynamic in these cases (Figure 2c). Such truncated growth was observed for Ge and Si nanowires grown by both VLS and VSS,[60,61] but has also been observed in many compound nanowire materials, including GaP,[60] GaAs,[62] and Al_2O_3.[63]

Compound semiconductor nanowires have also been studied extensively in more recent years. Compound nanowires require more complex gas supply systems capable of introducing two or more gas species simultaneously, which in some cases, should not mix before reaching the sample. Many important compound semiconductors, such as GaAs, involve toxic and dangerous gases in their synthesis, which necessitates the development of more advanced gas handling apparatus. Gas handling expertise from the semiconductor industry can however facilitate this development. The use of modern ETEM capabilities has allowed for *in situ* investigations of compound nanowire growth at precursor pressures much closer to comparable *ex situ* experiments than was possible for earlier studies of elemental semiconductors. Today, ETEM investigations of compound nanowire growth have been reported for GaP,[64] GaAs,[62] GaN,[65] InGaAs,[66] PdSe,[67] ZnTe,[68] CdTe,[68] ZnO,[69] and Al_2O_3.[63]

Similar to CNT synthesis, the phase, composition, and structure of the seed particle or droplet for different compound nanowire materials and synthesis conditions have been important unknowns for many years. With advancements in ETEM performance and complementary analysis capabilities, it is now possible to directly measure the droplet/particle composition during growth by EDX. Droplet composition for VLS-grown GaAs nanowires has been determined *in situ* along with its relationship to the growth parameters and resulting nanowire morphology, growth rate, and structure;[70] for compound $In_xGa_{1-x}As$ nanowires, these relationships were further correlated with the resulting nanowire composition.[66] For VSS-grown nanowires, the structure of the seed nanoparticle is often more efficiently determined from power spectra of high-resolution video frames, for instance for Cu-seeded GaP (Figure 2e).[71]

Several *in situ* studies have explored the process by which compound nanowire growth is initiated.[72,73] Once initiated, growth most often proceeds via a single nucleation event, followed by the completion of the layer before the next one nucleates (Figure 2d).[74] The dynamics of these nucleation and step-flow processes have been investigated in numerous studies. For GaAs, nucleation statistics of individual layers[75] and the evolution of the layer itself[76] have been investigated, as well as the relationship of these processes to the growth environment.[77] Size effects have also been explored, and it has been demonstrated that the step-flow process depends on nanowire diameter for small sizes.[78] For VSS-grown GaAs nanowires, similar nucleation and step-flow dynamics to VLS were observed for certain conditions, while an alternative growth parameter regime with negligible incubation time was also reported.[79]

Although the classical nucleation and step-flow process is typically observed, alternative processes with multiple steps growing simultaneously are also reported. For instance, for ZnTe nanowires grown from Au nanoparticles, VLS-grown nanowires typically exhibit single nucleation and step-flow events, while two-monolayer steps are observed for VSS growth;[68] this was attributed to lattice coincidence between the Au nanoparticle seed and the ZnTe nanowire. This observation differs somewhat from the case of VSS-grown GaAs, in which multiple steps occur due to multiple sequential nucleation events, but do not progress as a single two-layer step.[79] A similar observation was reported for VLS-grown GaN from Au droplets, potentially a consequence of low-N solubility even in a liquid catalyst.[80] On the other hand, double and triple bilayer step-flow growth have been reported for VLS-grown GaAs nanowires, and found to correlate with the occurrence of twin planes.[81] A more extreme case of multilayer growth with many simultaneously layers (up to 10) has been shown for InGaAs nanowires, and potentially attributed to compositional fluctuations during the growth process.[82]

The relationship between growth dynamics and nanowire crystal structure is an important topic for compound semiconductor nanowires. Unlike elemental semiconductors, which typically only exhibit diamond crystal structure with rare twin defects, compound semiconductor nanowires form both cubic zinc blende and hexagonal wurtzite crystal phases, with very frequent stacking defects. ETEM investigations have shown that stacking defects occurring during GaP nanowire growth cause a transient increase in the growth rate,[64] while twin defects in GaAs often result in multiple layers growing simultaneously.[81] The ability to tune the predominant crystal phase by tuning precursor pressures has also been shown *in*

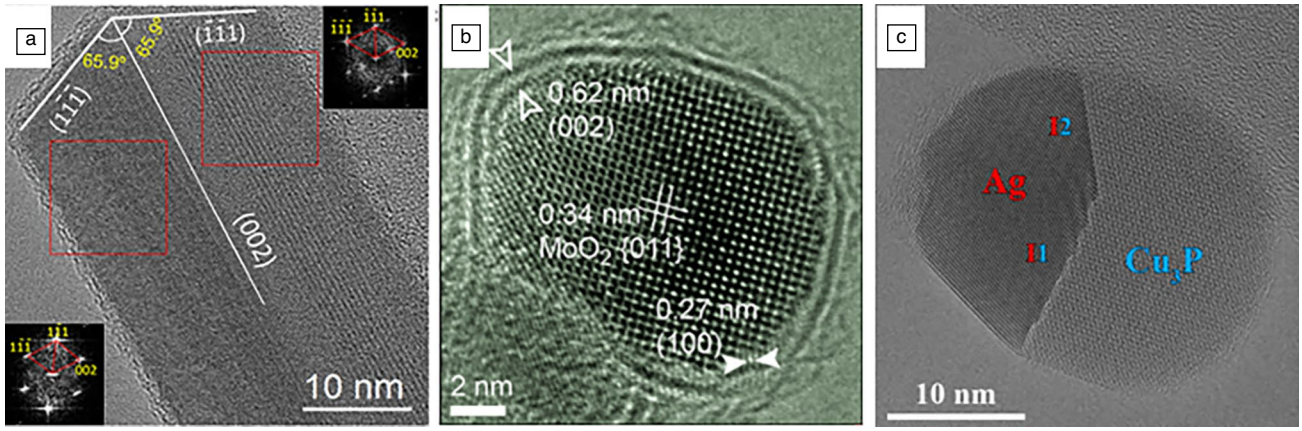

Figure 3. Crystal growth by *in situ* transformation of solids in reactive gas. (a) Growth of copper oxide nanowires from metallic Cu. Reprinted with permission from Reference 89. © 2014 American Chemical Society. (b) Surface sulfidation of a MoO_2 crystal to form MoS_2. Reprinted with permission from Reference 94. © 2018 American Chemical Society. (c) Transformation of Cu into Cu_3P by exposure to phosphine gas. Adapted with permission from Reference 95 under Creative Commons CC BY license.

situ,[70,74] consistent with *ex situ* results.[83] In some cases, the structure change is correlated with a change in droplet morphology for VLS growth, with larger droplets associated with higher prevalence of zinc blende;[74] this is especially apparent for GaAs nanowires seeded with Ga droplets.[84]

Finally, an unusual case is highlighted in which a liquid semiconductor acts as a catalyst for 1D semiconductor growth. Ge-catalyzed growth of ZnO has been demonstrated, accounting for not only solid straight nanowires, but also twisted nanowires and twisted hollow nanotubes. By controlling the addition of digermane in ETEM, a competition between growth and etching reactions during synthesis was identified, which could explain the variety of complex morphologies observed.[69]

Crystal growth by solid–vapor transformation

Crystal growth can also be performed via the reaction of a gas-phase precursor with a solid precursor deposited on the sample holder. The typical example of this type of process is oxidation, in which an oxide material is grown by reaction of a metal with oxygen or other oxidizing gas. Transformations of this type are distinguished from reactions such as catalysis where there is no net transfer of atoms from the gas to solid phase. They also differ fundamentally from catalyzed CNT and nanowire growth because the solid precursor is consumed in the process (although hybrid processes are also possible).

Studies of oxide formation in ETEM are widespread, especially for catalytic materials[85] and corrosion of structural materials[86] or in lithium batteries.[87] Numerous ETEM studies have also explored the synthesis of novel oxide nanostructures: for instance, a mechanism for forming hollow bimetallic nanoparticles has been investigated,[88] as well as a noncatalytic process for forming CuO nanowires from metallic Cu (**Figure 3**a).[89] A VLS-type process could also occur, as observed by reaction of oxygen with Al metal to form Al_2O_3 nanowires.[63] Residual oxygen or water in the vacuum could in some cases be sufficient to study oxide growth, but in modern ETEM experiments it is more common that oxygen gas or water is introduced directly to control the process. Similar transformation processes can also be studied in other compounds. The carburization process of iron to form Fe_5C_2, considered an active species for catalytic formation of some types of nanocarbons, has been investigated in ETEM using Fe nanoparticles exposed to CO.[90] The transformation of Fe into Fe_5C_2 is one step in the Fischer–Tropsch synthesis to convert coal into chemicals, but the investigation was also able to understand the nucleation and growth kinetics of the Fe_5C_2 itself.

Several studies have also investigated the formation of MoS_2, one of the most important of the transition-metal dichalcogenides, which have potential in (opto)electronic and catalytic applications.[91] Although most *in situ* TEM studies of MoS_2 involve the reaction of solid-state precursors, in some cases aided by the electron beam,[92] gas-phase synthesis has also been explored using H_2S together with a MoO_3 solid precursor. Heterogeneous nucleation of MoS_2 on the oxide precursor was observed, followed by layer-by-layer growth to form MoS_2 nanocrystals. The transformation from single- to multilayer crystals was found to correlate with reaction conditions such as temperature.[93] The formation of edge-terminated MoS_2 layers by a topotactic reaction was also later investigated using MoO_2 as a precursor together with H_2S (Figure 3b).[94] Because many of the important properties of MoS_2 and other transition-metal dichalcogenides arise from their edge sites, an understanding of the processes for forming crystals in this way is an important breakthrough.

A similar process has been used to explore the formation dynamics of Cu_3P by reaction of phosphine gas with Cu-Ag nanoparticles in an ETEM (Figure 3c).[95] Transition-metal phosphides are considered interesting as earth-abundant catalyst materials with superior thermal and chemical stability, while the inclusion of Ag enhances photocatalytic

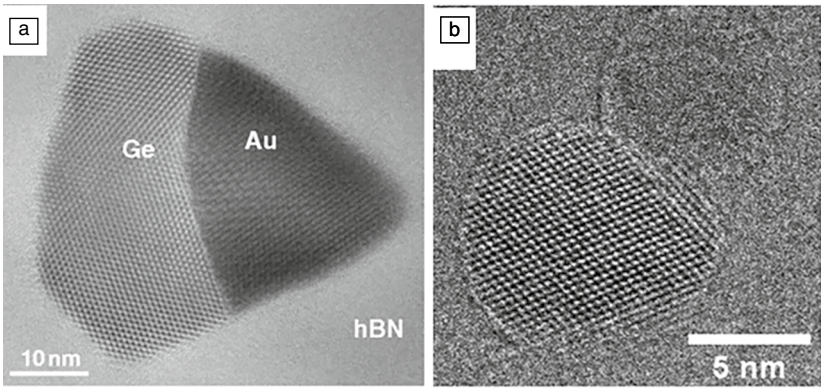

Figure 4. Crystal growth *in situ* on 2D substrates. (a) Au-catalyzed growth of Ge nanocrystals on hBN. Reprinted with permission from Reference 107 under Creative Commons CC BY license. (b) Direct nucleation and growth of Ge nanocrystals on graphene. Reprinted with permission from Reference 105. License number 5546450029554, © 2021 Wiley.

performance via band-edge tuning and efficient charge separation. The type of interface formed between the Cu_3P and Ag was found to depend on process conditions. This process can also be combined with a quasi-VSS type of process, whereby the formation of Cu_3P and GaP were simultaneously studied in combination with a Ag catalyst.[96] Similar hybrid synthesis processes can also be studied in other catalyzed CNT or nanowire investigations. As discussed, catalyst particles in many cases form compounds that are themselves interesting materials, and combinations of these compounds with the CNTs or semiconductors could have further potential applications. In some cases, with careful design of the synthesis process, it is possible to form compounds from catalyst particles that can then be integrated into the semiconductor to form complex hybrid systems.[97]

Direct nucleation and epitaxy

The previously discussed examples made use of a catalyst or solid precursor to initiate the growth studied. This has distinct technical advantages: because the approximate location at which growth will initiate is known, it is easier to follow nucleation and early growth stages, especially in high resolution. However, direct nucleation and growth on a crystalline or amorphous substrate are also possible. One of the earliest *in situ* studies involving crystal growth from a precursor gas in a modified TEM involved the deposition of metallic aluminum on SiO_2 substrate using trimethylamine alane as a precursor.[3] A similar process was used to study the growth of Ge islands on crystalline Si substrates using germane gas in a modified UHV TEM.[4,98,99] Weak beam imaging was used to observe the strain fields directly, to elucidate the role of stress in determining the shape of islands as they formed. It was demonstrated that islands grow on Si (001) in a cyclic mode with alternating periods of rapid and slow growth as dislocations are introduced.[4] At higher temperatures, relaxation occurs via dislocation glide,[100] while at lower temperatures, dislocations are incorporated directly during growth from edges on the substrate.[98] Nucleation, growth, and relaxation processes are more complicated on Si (111) substrates, with surface steps playing a critical role in relaxation, which occurs via different mechanisms depending on step direction and temperature.[99] The growth kinetics, nucleation and relaxation mechanism were also investigated in the presence of Ga surfactant.[101] Another study determined that coarsening of islands occurs even during growth.[102]

Epitaxial growth of SiGe thin films on Si substrates was investigated by a similar method using digermane and disilane as precursor gases.[103,104] For sufficiently low Ge composition, epilayers form that cover the Si structure, rather than islands. Relaxation occurs via the formation of misfit dislocations, and the effect of the surface on the velocity by which these dislocations propagate through the film has been measured *in situ*.[103] In particular, the presence of a native oxide on the substrate enhances dislocation propagation. Moreover, the interaction between dislocations has also been investigated, with the conclusion that dislocation interaction blocks their movement for thinner films, while above a certain thickness this effect is significantly decreased.[104]

Integration of 2D materials with semiconductors and metals is an important step in their application, and understanding the crystal growth process can enable this development. Because there are relatively few ways to access the information needed to understand nucleation on 2D materials, ETEM has an important role (**Figure** 4). For instance, the formation of Ge nanocrystals on graphene has been explored.[105] Nucleation and growth kinetics were determined; it was reported that nucleation on clean graphene was challenging and enabled by a two-step nucleation/annealing procedure. Moreover, an Ostwald ripening process was important to the growth due to the weak interaction between the Ge and graphene, which nevertheless ultimately exhibited an epitaxial relationship. More exotic combinations of metal nanocrystal growth on 2D materials have been explored, including Au, Ti, and Nb thermally evaporated grown on MoS_2, WS_2, WSe_2, and graphene.[106]

Integration of 3D nanocrystals on 2D materials has also been studied *in situ* by a catalytic process,[107] similar to those described for CNTs and nanowires above. Epitaxial growth of Ge and Si on graphene was achieved using Au and Ag catalysts, yielding a significantly easier-to-control process for combining these materials. In this case, the solid metal nanoparticles align with the substrate, promoting epitaxial nucleation of the semiconductor on the graphene surface.

Summary, conclusions, outlook

This article reviews the background and latest progress in understanding materials synthesis using ETEM, with an emphasis on elucidating growth mechanisms in novel nanostructure materials. Gas-phase electron microscopy has contributed enormously to understanding the fundamental mechanisms by which nanocrystals form and the relationships between synthesis conditions and resulting materials properties. Although breakthrough insights have been afforded by *in situ* TEM experiments over many decades, recent developments in performance, resolution, and analysis capabilities of ETEM instruments have particularly driven a wealth of studies. Challenges remain, for instance, in ensuring that the *in situ* environment is sufficiently representative of a conventional synthesis process for the insights to be broadly relevant. In order for insights afforded by ETEM to be applied to conventional synthesis situations, it is essential to ensure that the *in situ* environment is sufficiently similar. However, modern closed-cell gas holders and dedicated ETEMs have largely closed the "pressure gap," and realistic temperatures are now routinely achievable. Such advancements are also critical to ensuring that quantitative, reproducible data on growth mechanisms can be extracted. Another challenge is to fully understand the way in which the electron beam affects the sample and environment during a dynamic process—beam effects can never be fully excluded in a situation where the electron beam by definition must interact with the material as it forms. Here as well, substantial progress is being made in understanding how to account for (and compensate for) these effects. It can be anticipated that ETEM will play an increasingly important role in the development of new novel materials and in addressing fundamental questions in their synthesis, nucleation, and crystal growth.

Conflict of interest

The corresponding author states that there is no conflict of interest.

Open Access

References

1. N. Petkov, *Int. Sch. Res. Notices* **2013**, 893060 (2013)
2. J.M. Gibson, M.Y. Lanzerotti, *Ultramicroscopy* **31**, 29 (1989)
3. J. Drucker, R. Sharma, K. Weiss, *J. Appl. Phys.* **77**, 2846 (1995)
4. F.K. LeGoues, M.C. Reuter, J. Tersoff, M. Hammar, R.M. Tromp, *Phys. Rev. Lett.* **73**(2), 300 (1994)
5. J. Li, F.L. Deepak, *Chem. Rev.* **122**, 16911 (2022)
6. J. Jinschek, P. Crozier, *MRS Bull.* **48**(8) (2023)
7. M. Tornberg, C.B. Maliakkal, D. Jacobsson, R. Wallenberg, K.A. Dick, *Microsc. Microanal.* **28**, 1484 (2022)
8. G. Zhou, K. Unocic, C. Wang, Z. Shan, S. Haigh, J. Yang, *MRS Bull.* **48**(8) (2023)
9. M. Willinger, *MRS Bull.* **48**(8) (2023)
10. S. Iijima, *Nature* **354**, 56 (1992)
11. R. Sharma, Z. Iqbal, *Appl. Phys. Lett.* **84**, 990 (2004)
12. S. Helveg, C. López-Cartes, J. Sehested, P.L. Hansen, B.S. Clausen, J.R. Rostrup-Nielsen, F. Abild-Pedersen, J.K. Nørskov, *Nature* **427**, 426 (2004)
13. R. Sharma, P. Rez, M.M.J. Treacy, J. Stuart, *J. Electron Microsc.* **54**, 231 (2005)
14. V. Balakrishnan, M. Bedewy, E.R. Meshot, S.W. Pattinson, E.S. Polsen, F. Laye, D.N. Zakharov, E.A. Stach, A.J. Hart, *ACS Nano* **10**, 11496 (2016)
15. R. Sharma, E. Moore, P. Rez, M.M. Treacy, *Nano Lett.* **9**, 689 (2009)
16. M. Bedewy, B. Viswanath, E.R. Meshot, D.N. Zakharov, E.A. Stach, A.J. Hart, *Chem. Mater.* **28**, 3804 (2016)
17. R. Rao, R. Sharma, F. Abild-Pedersen, J.K. Nørskov, A.R. Harutyunyan, *Sci. Rep.* **4**, 6510 (2014)
18. M. Picher, P.A. Lin, J.L. Gomez-Ballesteros, P.B. Balbuena, R. Sharma, *Nano Lett.* **14**, 6104 (2014)
19. K. Dembélé, M. Bahri, G. Melinte, C. Hirlimann, A. Berliet, S. Maury, A.-S. Gay, O. Ersen, *ChemCatChem* **10**, 4004 (2018)
20. E. Pigos, E.S. Penev, M.A. Ribas, R. Sharma, B.I. Yakobson, A.R. Harutyunyan, *ACS Nano* **5**, 10096 (2011)
21. H. Yoshida, S. Takeda, T. Uchiyama, H. Kohno, Y. Homma, *Nano Lett.* **8**, 2082 (2008)
22. D.M. Tang, C. Liu, W.J. Yu, L.L. Zhang, P.X. Hou, J.C. Li, F. Li, Y. Bando, D. Golberg, H.M. Cheng, *ACS Nano* **8**, 292 (2014)
23. X. Feng, S.W. Chee, R. Sharma, K. Liu, X. Xie, Q. Li, S. Fan, K. Jiang, *Nano Res.* **4**, 767 (2011)
24. M. Bahri, K. Dembélé, C. Sassoye, D.P. Debecker, S. Moldovan, A.S. Gay, Ch. Hirlimann, C. Sanchez, O. Ersen, *Nanoscale* **10**, 14957 (2018)
25. C.T. Wirth, B.C. Bayer, A.D. Gamalski, S. Esconjauregui, R.S. Weatherup, C. Ducati, C. Baehtz, J. Robertson, S. Hofmann, *Chem. Mater.* **24**, 4633 (2012)
26. S. Mazzucco, Y. Wang, M. Tanase, M. Picher, K. Li, Z. Wu, S. Irle, R. Sharma, *J. Catal.* **319**, 54 (2014)
27. Y. Kohigashi, H. Yoshida, Y. Homma, S. Takeda, *Appl. Phys. Lett.* **105**, 073108 (2014)
28. S. Hofmann, R. Sharma, C. Ducati, G. Du, C. Mattevi, C. Cepek, M. Cantoro, S. Pisana, A. Parvez, F. Cervantes-Sodi, A.C. Ferrari, R. Dunin-Borkowski, S. Lizzit, L. Petaccia, A. Goldoni, J. Robertson, *Nano Lett.* **7**, 602 (2007)
29. S. Hofmann, R. Blume, C.T. Wirth, M. Cantoro, R. Sharma, C. Ducati, M. Hävecker, S. Zafeiratos, P. Schnoerch, A. Oestereich, D. Teschner, M. Albrecht, A. Knop-Gericke, R. Schlögl, J. Robertson, *J. Phys. Chem. C* **113**, 1648 (2009)
30. X. Huang, R. Farra, R. Schlogl, M.G. Willinger, *Nano Lett.* **19**, 5380 (2019)
31. Y. Lyu, P. Wang, D. Liu, F. Zhang, T.P. Senftle, G. Zhang, Z. Zhang, J. Wang, W. Liu, *Small Methods* **6**, 2200235 (2022)
32. Y. Wang, L. Qiu, L. Zhang, D.M. Tang, R. Ma, Y. Wang, B. Zhang, F. Ding, C. Liu, H.M. Cheng, *ACS Nano* **14**, 16823 (2020)
33. P.A. Lin, J.L. Gomez-Ballesteros, J.C. Burgos, P.B. Balbuena, B. Natarajan, R. Sharma, *J. Catal.* **349**, 149 (2017)
34. J.L. Maurice, D. Pribat, Z. He, G. Patriarche, C.S. Cojocaru, *Carbon* **79**, 93 (2014)
35. L. Zhang, M. He, T.W. Hansen, J. Kling, H. Jiang, E.I. Kauppinen, A. Loiseau, J.B. Wagner, *ACS Nano* **11**, 4483 (2017)
36. X. Zhang, D. Tian, F. Yang, H. Zhao, W.M. Lau, R. Wang, *Adv. Mater. Interfaces* **9**, 2200334 (2022)
37. M. He, H. Jiang, B. Liu, P.V. Fedotov, A.I. Chernov, E.D. Obraztsova, F. Cavalca, J.B. Wagner, T.W. Hansen, I.V. Anoshkin, E.A. Obraztsova, A.V. Belkin, E. Sairanen, A.G. Nasibulin, J. Lehtonen, E.I. Kauppinen, *Sci. Rep.* **3**, 1460 (2013)
38. R. Ma, L. Qiu, L. Zhang, D.M. Tang, Y. Wang, B. Zhang, F. Ding, C. Liu, H.M. Cheng, *ACS Nano* **16**, 16574 (2022)
39. H. Fan, L. Qiu, A. Fedorov, M.G. Willinger, F. Ding, X. Huang, *ACS Nano* **15**, 17895 (2021)
40. Y. Wang, L. Qiu, L. Zhang, D.M. Tang, R. Ma, C.L. Ren, F. Ding, C. Liu, H.M. Cheng, *Sci. Adv.* **8**, eabo5686 (2022)
41. C. Jia, Z. Lin, Y. Huang, X. Duan, *Chem. Rev.* **119**, 9074 (2019)
42. N. Quan, J. Kang, C.Z. Ning, P. Yang, *Chem. Rev.* **119**, 9153 (2019)
43. E. Barrigón, M. Heurlin, Z. Bi, B. Monemar, L. Samuelson, *Chem. Rev.* **119**, 9170 (2019)
44. F.M. Ross, *Rep. Prog. Phys.* **73**, 114501 (2010)
45. Y. Wu, P. Yang, *J. Am. Chem. Soc.* **123**, 3165 (2001)

46. S. Kodambaka, J. Tersoff, M.C. Reuter, F.M. Ross, *Phys. Rev. Lett.* **96**, 096105 (2006)
47. J.B. Hannon, S. Kodambaka, F.M. Ross, R.M. Tromp, *Nature* **440**, 69 (2006)
48. S. Kodambaka, J.B. Hannon, R.M. Tromp, F.M. Ross, *Nano Lett.* **6**, 1292 (2006)
49. F.M. Ross, J. Tersoff, M.C. Reuter, *Phys. Rev. Lett.* **95**, 146104 (2005)
50. P. Madras, E. Dailey, J. Drucker, *Nano Lett.* **9**, 3826 (2009)
51. K.W. Schwarz, J. Tersoff, S. Kodambaka, F.M. Ross, *Phys Rev Lett.* **113**, 055501 (2014)
52. S. Kodambaka, J. Tersoff, M.C. Reuter, F.M. Ross, *Science* **316**, 729 (2007)
53. C.Y. Wen, M.C. Reuter, J. Bruley, J. Tersoff, S. Kodambaka, E.A. Stach, F.M. Ross, *Science* **326**, 1247 (2009)
54. C.Y. Wen, M.C. Reuter, J. Tersoff, E.A. Stach, F.M. Ross, *Nano Lett.* **10**, 514 (2010)
55. S. Hofmann, R. Sharma, C.T. Wirth, F. Cervantes-Sodi, C. Ducati, T. Kasama, R.E. Dunin-Borkowski, J. Drucker, P. Bennett, J. Robertson, *Nat. Mater.* **7**, 372 (2008)
56. B.J. Kim, J. Tersoff, S. Kodambaka, M.C. Reuter, E.A. Stach, F.M. Ross, *Science* **322**, 1070 (2008)
57. B.J. Kim, C.Y. Wen, J. Tersoff, M.C. Reuter, E.A. Stach, F.M. Ross, *Nano Lett.* **12**, 5867 (2012)
58. C.Y. Wen, J. Tersoff, M.C. Reuter, E.A. Stach, F.M. Ross, *Phys. Rev. Lett.* **105**, 195502 (2010)
59. Y.C. Chou, F. Panciera, M.C. Reuter, E.A. Stach, F.M. Ross, *Chem. Commun.* **52**, 5686 (2016)
60. C.Y. Wen, J. Tersoff, K. Hillerich, M.C. Reuter, J.H. Park, S. Kodambaka, E.A. Stach, F.M. Ross, *Phys. Rev. Lett.* **107**, 025503 (2011)
61. A.D. Gamalski, C. Ducati, S. Hofmann, *J. Phys. Chem. C* **115**, 4413 (2011)
62. M. Tornberg, C.B. Maliakkal, D. Jacobsson, K.A. Dick, J. Johansson, *J. Phys. Chem. Lett.* **11**, 2949 (2020)
63. S.H. Oh, M.F. Chisholm, Y. Kauffmann, W.D. Kaplan, W. Luo, M. Rühle, C. Scheu, *Science* **330**(6003), 489 (2010)
64. Y.C. Chou, K. Hillerich, J. Tersoff, M.C. Reuter, K.A. Dick, F.M. Ross, *Science* **343**, 281 (2014)
65. E.A. Stach, P.J. Pauzauskie, T. Kuykendall, J. Goldberger, R. He, P. Yang, *Nano Lett.* **3**, 867 (2003)
66. R. Sjökvist, D. Jacobsson, M. Tornberg, R. Wallenberg, E.D. Leshchenko, J. Johansson, K.A. Dick, *J. Phys. Chem. Lett.* **12**(31), 7590 (2021)
67. M. Song, J. Lee, B. Wang, B.A. Legg, S. Hu, J. Chun, D. Li, *Nanoscale* **11**, 5874 (2019)
68. E. Bellet-Amalric, F. Panciera, G. Patriarche, L. Travers, M. den Hertog, J.C. Harmand, F. Glas, J. Cibert, *ACS Nano* **16**(3), 4397 (2022)
69. T. Pham, S. Kommandur, H. Lee, D. Zakharov, M.A. Filler, F.M. Ross, *Nanotechnology* **32**, 075603 (2021)
70. C.B. Maliakkal, D. Jacobsson, M. Tornberg, A.R. Persson, J. Johansson, R. Wallenberg, K.A. Dick, *Nat. Commun.* **10**, 4577 (2019)
71. T. Hu, M.S. Seifner, M. Snellman, D. Jacobsson, M. Sedrpooshan, P. Ternero, M.E. Messing, K.A. Dick, *Small Struct.* 230011 (2023)
72. C.B. Maliakkal, D. Jacobsson, M. Tornberg, K.A. Dick, *Nanotechnology* **33**, 105607 (2021)
73. R.E. Diaz, R. Sharma, K. Jarvis, Q. Zhang, S. Mahajan, *J. Cryst. Growth* **341**(1), 1 (2012)
74. D. Jacobsson, F. Panciera, J. Tersoff, M.C. Reuter, S. Lehmann, S. Hofmann, K.A. Dick, F.M. Ross, *Nature* **531**, 317 (2016)
75. F. Glas, F. Panciera, J.C. Harmand, *Phys. Status Solidi Rapid. Res. Lett.* **16**, 2100647 (2022)
76. J.C. Harmand, G. Patriarche, F. Glas, F. Panciera, I. Florea, J.L. Maurice, L. Travers, Y. Ollivier, *Phys. Rev. Lett.* **121**, 166101 (2018)
77. C.B. Maliakkal, E.K. Mårtensson, M.U. Tornberg, D. Jacobsson, A.R. Persson, J. Johansson, L.R. Wallenberg, K.A. Dick, *ACS Nano* **4**, 3868 (2020)
78. M. Marnauza, M. Tornberg, E.K. Martensson, D. Jacobsson, K.A. Dick, *Nanoscale Horiz.* **8**, 291 (2023)
79. C.B. Maliakkal, M. Tornberg, D. Jacobsson, S. Lehmann, K.A. Dick, *Nanoscale Adv.* **3**, 5928 (2021)
80. A.D. Gamalski, J. Tersoff, E.A. Stach, *Nano Lett.* **16**, 2283 (2016)
81. M. Tornberg, R. Sjökvist, K. Kumar, C.R. Andersen, C.B. Maliakkal, D. Jacobsson, K.A. Dick, *ACS Nanosci. Au* **2**(1), 49 (2022)
82. R. Sjökvist, M. Tornberg, M. Marnauza, D. Jacobsson, K.A. Dick, *ACS Nanosci. Au* **2**(6), 539 (2022)
83. S. Lehmann, D. Jacobsson, K.A. Dick, *Nanotechnology* **26**, 301001 (2015)
84. F. Panciera, Z. Baraissov, G. Patriarche, V.G. Dubrovskii, F. Glas, L. Travers, U. Mirsaidov, J.C. Harmand, *Nano Lett.* **20**, 1669 (2020)
85. B. He, Y. Zhang, X. Liu, L. Chen, *ChemCatChem* **12**, 1853 (2020)
86. M.G. Burke, G. Bertali, E. Prestat, F. Scenini, S.J. Haigh, *Ultramicroscopy* **176**, 46 (2017)
87. Y. Li, X. Li, J. Chen, C. Cai, W. Tu, J. Zhao, Y. Tang, L. Zhang, G. Zhou, J. Huang, *Adv. Funct. Mater.* **32**, 2203233 (2022)
88. W. Xia, Y. Yang, Q. Meng, Z. Deng, M. Gong, J. Wang, D. Wang, Y. Zhu, L. Sun, F. Xu, J. Li, H.L. Xin, *ACS Nano* **12**, 7866 (2018)
89. S. Rackauskas, H. Jiang, J.B. Wagner, S.D. Shandakov, T.W. Hansen, E.I. Kauppinen, A.G. Nasibulin, *Nano Lett.* **14**, 5810 (2014)
90. X. Liu, C. Zhang, Y. Li, J.W. Niemantsverdriet, J.B. Wagner, T.W. Hansen, *ACS Catal.* **7**, 4867 (2017)
91. V.P. Kumar, D.K. Panda, *ECS J. Solid State Sci. Technol.* **11**, 033012 (2022)
92. Y. Zhu, D. Yuan, H. Zhang, T. Xu, L. Sun, *Nano Res.* **14**, 1650 (2021)
93. L.P. Hansen, E. Johnson, M. Brorson, S. Helveg, *J. Phys. Chem. C* **118**(39), 22768 (2014)
94. C. Dahl-Petersen, M. Šarić, M. Brorson, P.G. Moses, J. Rossmeisl, J. Vang Lauritsen, S. Helveg, *ACS Nano* **12**, 5351 (2018)
95. M.S. Seifner, M. Snellman, O.A. Makgae, K. Kumar, D. Jacobsson, M. Ek, K. Deppert, M.E. Messing, K.A. Dick, *J. Am. Chem. Soc.* **144**(1), 248 (2022)
96. M.S. Seifner, T. Hu, M. Snellman, D. Jacobsson, K. Deppert, M.E. Messing, K.A. Dick, *ACS Nano* **17**, 7674 (2023)
97. F. Panciera, Y.-C. Chou, M.C. Reuter, D. Zakharov, E.A. Stach, S. Hofmann, F.M. Ross, *Nat. Mater.* **14**, 820 (2015)
98. F.K. LeGoues, J. Tersoff, M.C. Reuter, M. Hammar, R. Tromp, *Appl. Phys. Lett.* **67**, 2317 (1995)
99. F.K. LeGoues, M. Hammar, M.C. Reuter, R.M. Tromp, *Surf. Sci.* **349**, 249 (1996)
100. M. Hammar, F.K. LeGoues, J. Tersoff, M.C. Reuter, R.M. Tromp, *Surf. Sci.* **349**, 129 (1996)
101. A. Portavoce, M. Kammler, R. Hull, M.C. Reuter, M. Copel, F.M. Ross, *Phys. Rev. B* **70**, 195306 (2004)
102. F.M. Ross, J. Tersoff, R.M. Tromp, *Phys. Rev. Lett.* **80**, 984 (1988)
103. E.A. Stach, R. Hull, R.M. Tromp, M.C. Reuter, M. Copel, F.K. LeGoues, J.C. Bean, *J. Appl. Phys.* **83**, 1931 (1998)
104. E.A. Stach, R. Hull, R.M. Tromp, F.M. Ross, M.C. Reuter, J.C. Bean, *Philos. Mag. A* **80**, 2159 (2000)
105. T. Mamoudou Diallo, M.R. Aziziyan, R. Arvinte, J.-C. Harmand, G. Patriarche, C. Renard, S. Fafard, R. Arès, A. Boucherif, *Small* **18**, 2101890 (2022)
106. K. Reidy, J. Dahl Thomsen, H.Y. Lee, V. Zarubin, Y. Yu, B. Wang, T. Pham, P. Periwal, F.M. Ross, *Nano Lett.* **22**, 5849 (2022)
107. P. Periwal, J. Dahl Thomsen, K. Reidy, G. Varnavides, D.N. Zakharov, L. Gignac, M.C. Reuter, T.J. Booth, S. Hofmann, F.M. Ross, *Appl. Phys. Rev.* **7**, 031402 (2020)

Kimberly A. Dick is a professor of materials science at the Centre for Analysis and Synthesis in the Department of Chemistry at Lund University, Sweden. She is a member of the Royal Swedish Academy of Engineering Sciences. She received her PhD degree in physics in 2007, following a Bachelor of Science in chemical physics in 2003. Her research involves the crystal growth of novel semiconductor nanomaterials, with particular focus on understanding growth processes using *in situ* transmission electron microscopy. Dick can be reached by email at kimberly.dick@ftf.lth.se.